④

OFFICE OF NAVAL RESEARCH

Contract N00014-80-K-0852

R&T Code______________

Technical Report No. 42

Forbidden Electron Attachement in O_2

By

H. Sambe and D. E. Ramaker

Prepared for Publication
in the
Physical Review B

George Washington University
Department of Chemistry
Washington, D.C. 20052

December, 1988

SECURITY CLASSIFICATION OF THIS PAGE

REPORT DOCUMENTATION PAGE

1a. REPORT SECURITY CLASSIFICATION
Unclassified

1b. RESTRICTIVE MARKINGS

2a. SECURITY CLASSIFICATION AUTHORITY

2b. DECLASSIFICATION / DOWNGRADING SCHEDULE

3. DISTRIBUTION / AVAILABILITY OF REPORT
Approved for Public Release, distribution Unlimited.

4. PERFORMING ORGANIZATION REPORT NUMBER(S)
Technical Report #42

5. MONITORING ORGANIZATION REPORT NUMBER(S)

6a. NAME OF PERFORMING ORGANIZATION
Dept. of Chemistry
George Washington Univ.

6b. OFFICE SYMBOL *(If applicable)*

7a. NAME OF MONITORING ORGANIZATION
Office of Naval Research (Code 413)

6c. ADDRESS *(City, State, and ZIP Code)*
Washington, D.C. 20052

7b. ADDRESS *(City, State, and ZIP Code)*
Chemistry Program
800 N. Quincy Street
Arlington, VA 22217

8a. NAME OF FUNDING / SPONSORING ORGANIZATION
Office of Naval Research

8b. OFFICE SYMBOL *(If applicable)*

9. PROCUREMENT INSTRUMENT IDENTIFICATION NUMBER
Contract N00014-80-K-0852

8c. ADDRESS *(City, State, and ZIP Code)*
Chemistry Program
800 North QUINCY, Arlington, VA 22217

10. SOURCE OF FUNDING NUMBERS

PROGRAM ELEMENT NO.	PROJECT NO.	TASK NO.	WORK UNIT ACCESSION NO.
61153 N		PP 013-08-01	NR 056-681

11. TITLE *(Include Security Classification)*
Forbidden Electron Attachment in O_2 (Uncl.)

12. PERSONAL AUTHOR(S)
H. Sambe and D. E. Ramaker

13a. TYPE OF REPORT
Interim Technical

13b. TIME COVERED
FROM ________ TO ________

14. DATE OF REPORT *(Year, Month, Day)*
December 1988

15. PAGE COUNT
24

16. SUPPLEMENTARY NOTATION
Prepared for publication in Physical Review B

17. COSATI CODES

FIELD	GROUP	SUB-GROUP

18. SUBJECT TERMS *(Continue on reverse if necessary and identify by block number)*
Dissociative attachment, desorption, forbidden transitions, dissociation, oxygen.

19. ABSTRACT *(Continue on reverse if necessary and identify by block number)*

The electron stimulated O^- desorption yield from condensed 0_2 exhibits three peaks around 7, 8.5, and 13 eV, while that from 0_2 gas shows only the 7-eV peak . The 7-eV peak is know to arise from the $O_2^-(1\pi_u^{-1}1\pi_g^{2})^2\Pi_u$ compound state. In this paper, the 8.5- and 13-eV peaks are shown to arise from the $O_2^-(3\sigma_g^{-1}1\pi_g^{2})\ ^2\Sigma_g^+$ and $O_2^-(2\sigma_u^{-1}1\pi_g^{2})^2\Sigma_u^+$ compound states, respectively.

The absence of the 8.5- and 13-eV peaks in the gas-phase spectrum is shown to be due to a $\Sigma^-\leftrightarrow/\rightarrow\Sigma^+$ selection rule, which is valid only in the highly symmetrical environment of the gas phase.

20. DISTRIBUTION / AVAILABILITY OF ABSTRACT
☒ UNCLASSIFIED/UNLIMITED ☒ SAME AS RPT. ☐ DTIC USERS

21. ABSTRACT SECURITY CLASSIFICATION
Unclassified

22a. NAME OF RESPONSIBLE INDIVIDUAL
Dr. David L. Nelson

22b. TELEPHONE *(Include Area Code)*
(202) 696-4410

22c. OFFICE SYMBOL

DD FORM 1473, 84 MAR

83 APR edition may be used until exhausted.
All other editions are obsolete.

SECURITY CLASSIFICATION OF THIS PAGE
Unclassified

88 12 035

I. INTRODUCTION

In collisions of electrons with molecules, an electron may be attached to a molecule forming a temporary negative ion or a negative compound state. The production of this compound state is governed by certain selection rules. The selection rules are: (1) An allowed compound state must have either $|S-1/2|$ or $|S+1/2|$ total spin, when the target molecule has total spin S; (2) it should have an electronic configuration which differs by less than three-electron excitations with respect to the initial state (i.e., the target molecule plus an incident electron); (3) it must not have Σ^- (Σ^+) symmetry, if the target molecule is linear and has Σ^+ (Σ^-) symmetry. The last selection rule has been established just recently and has been called the σ^- selection rule.[1] When either of the three selection rules are not satisfied, we use the term, forbidden electron attachment, by analogy with forbidden optical transitions.

Compound states which are forbidden in the gas phase may not be forbidden in the solid phase, because of distortion of the local symmetry. Although the selection rules involving spin symmetry and number of electron excitations may persist in the solid phase, the rule involving cylindrical symmetry of linear molecules (or the σ^- selection rule) may relax in the solid phase. In fact, this breakdown of cylindrical symmetry has been clearly observed in optical transitions.[2] In this paper, we study O_2 molecular systems in the gas and solid phases and

oxygen

over

sigma

identify, for the first time, the compound states which are forbidden by the σ selection rule. (mjm)

In Sec. II, we analyze some experimental data previously published in the literature. Our findings are summarized in Table I. In Sec. III, various properties of the lower-lying O_2^- compound states are predicted utilizing empirical methods. These properties are summarized in Table VII. In Sec. IV, we identify the forbidden compound states by comparing experimental (Table I) and theoretical (Table VII) results. Finally in Sec. V, we review previous work.

II. EXPERIMENTAL RESULTS

A. Energy dependence of the O^- yields

Figure 1 shows electron stimulated O^- desorption yields from various samples (O_2/W, O_2/Pt, and O_2 gas) as a function of the incident electron energy. These O^- yield curves are reproduced from figures previously published in the literature.[3-6] The relative magnitudes of these curves do not represent the actual relative O^- yields. For example, the O^- yield from O_2 gas (dotted curve) is arbitrarily normalized to the peak of the O_2/Pt curve for comparison. For the O_2/W data,[6] a polycrystalline W ribbon was dosed with 10 L (Langmuirs, $1L=10^{-6}$ Torr Sec) of O_2 at room temperature. All three O_2/Pt samples[5,6] were prepared by condensing O_2 gas on a polycrystalline Pt ribbon at 20 K with a constant O_2 dosage. The estimated O_2 film thickness is 3 monolayers (ML) for all three Pt samples. Two of the three curves for O_2/Pt are measured with retarding potentials (V_R=-1.5 and -1.8 eV) against the outgoing O^- ions. The V_R=-1.8 eV retarding potential, for example, discriminates O^- ions whose kinetic energies outside the condensed film are less than 1.8 eV. The shaded area shows our estimated contribution due to the direct process, which we shall discuss later. Figure 2 shows the OH^- yield from C_6H_{14}(1ML)/O_2(3ML)/Pt and the $O_2 \cdot O^-$ and O_2^- yields from $(O_2)_n$ cluster. These curves are reproduced from Refs. 6 and 7 respectively. The O^- yield from O_2 gas (dotted curve) is shown again for comparison.

The O^- ions from O_2 are generated by the reaction

$$e^- + O_2 \rightarrow O_2^- \rightarrow O + O^- , \qquad (1)$$

so that maxima in the O^- yield curve reflect the positions of O_2^- compound states. The OH^- yields from C_nH_{2n+2}/O_2 also reflect the positions of O_2^- compound states, because the OH^- ions are generated by two steps; namely, reaction (1) followed by

$$O^- + C_nH_{2n+2} \rightarrow OH^- + C_nH_{2n+1} , \qquad (2)$$

according to Sanche and Parenteau.[4] Similarly, $O_2 \cdot O^-$ and O_2^- ions from O_2 clusters are generated via the initial step,

$$e^- + (O_2)_n \rightarrow (O_2)_{n-1} \cdot O_2^- . \qquad (3)$$

Therefore, the $O_2 \cdot O^-$ and O_2^- yield curves also reflect the positions of O_2^- compound states.

Figures 1 and 2 exhibit three peaks around 7, 8.5, and 13 eV as indicated in the two figures. The 8.5-eV peak in $(O_2)_n$ curves (Fig. 2) has been interpreted as a shift of the 7-eV state due to the polarization of the $(O_2)_n$ cluster.[7] Also the 8.5-eV peak in O_2/Pt curves (Fig. 1) was not ascribed to another compound state.[8] In this work, we attribute the 8.5-eV peak to another O_2^- compound state, based on the following four reasons: (1) Any polarization of the $(O_2)_n$ clusters should shift the 7-eV peak to lower energy, contrary to that observed. (2) The peak position of the 8.5-eV feature does not shift to higher energy, when the retarding potential is increased from -1.5 to -1.8 eV. In addition, there is an indication of a shoulder around 7 eV in the O_2/Pt(V_R=-1.5eV) curve, suggesting that the 7-eV peak has not been shifted. (3) All ion-yield curves measured without retarding potentials, except the O^- yield curve from gaseous O_2, indicate the presence of the 8.5-eV feature. In fact, the 8.5-eV feature dominates in the O_2^--$(O_2)_n$ curve of Fig. 2. (4) Theory predicts three O_2^- compound states in the energy range from 7 to 15 eV, which can dissociate into an O+O^- limit. To sum up, the 7-, 8.5-, and 13-eV features we believe to arise from three different O_2^- compound states.

As seen in Figs. 1 and 2, the relative intensities of the three features depend strongly on the structure of the sample (such as the O_2 layer thickness, substrate, and cluster size), the detected ions (O^-, O_2^-, $O_2 \cdot O^-$, or OH^-), and the detection angle of the ions. However, to establish the nature of the forbidden electron attachment, analysis of these intensities is not essential. The only fact which is used in this work is that both the 8.5- and 13-eV features are absent (or negligible relative to the 7-eV feature) in the O^- yield curve of gaseous O_2 (see Figs. 1 and 2).

B. O^- kinetic energy distributions

Figure 3 shows the kinetic energy distributions of the O^- ions from O_2(3ML)/Pt measured at various incident electron energies (E_i=5.7, 7.7, 12, and 13 eV). These data were obtained by Azria *et al.*[8] with an electron-energy resolution of 0.3 eV and an ion-energy resolution of 0.5 eV. The relative O^- kinetic energy (E_{rel}) (the absolute scale of the O^- kinetic energy was not determined) is measured with respect to the peak energy of the E_i=5.7eV curve. The three symbols in horizontal bars (closed and open circles and open triangle) indicate three different contributions, which will be described later. The horizontal bar with a symbol indicates the possible range of the peak position for each contribution. In Fig. 4, these peak-position ranges are plotted as a function of the incident electron energy, E_i. The broken straight lines are given by the equation,

$$E_{rel} = (E_i - E_d)/2 - 1.03 \text{ (eV)} , \qquad (4)$$

where E_d is the relevant $O+O^-$ dissociation limit measured from the O_2 ground state (v=0). The E_d=3.65, 5.62, and 7.84 eV correspond to the lowest three dissociation limits, $O(^3P)+O^-(^2P)$, $O(^1D)+O^-(^2P)$, and $O(^1S)+O^-(^2P)$, respectively. The O^- kinetic energy (E_{abs}) from O_2 gas is given by

$$E_{abs} = (E_i - E_d)/2 \ , \qquad (5)$$

where E_i and E_d have the same meanings as those of Eq. (4). The constant shift (1.03 eV) of E_{rel} with respect to E_{abs} arises from the artificial choice of the zero of energy for E_{rel} (i.e., $E_{rel}=0$ for $E_i=5.7$eV and $E_d=3.65$eV).

As seen in Fig. 4, the features denoted by closed circles fit well on the straight line with $E_d=3.65$ eV, indicating that they arise from the process,

$$e^- + O_2(^3\Sigma_g^-) \rightarrow O_2^- \rightarrow O(^3P) + O^-(^2P) \ . \qquad (6)$$

Similarly, the features with open circles fit well on the line with $E_d=5.62$eV, indicating that they arise from the process,

$$e^- + O_2(^3\Sigma_g^-) \rightarrow O_2^- \rightarrow O(^1D) + O^-(^2P) \ . \qquad (7)$$

On the other hand, the features with open triangles do not fit on any of the lines. These features have been previously ascribed to the multiple scattering process,[5] that is,

$$e^- + O_2(^3\Sigma_g^-) \rightarrow O_2^* + e^{-\prime} \qquad (8)$$

followed by

$$e^{-\prime} + O_2(^3\Sigma_g^-) \rightarrow O_2^- \rightarrow O(^3P) + O^-(^2P) \ . \qquad (9)$$

The above analysis supports this interpretation. A good fit to theory for the closed and open circles suggests that no significant amount of momentum is transferred to the O_2 lattice when the O^- desorbs from the surface. A similar conclusion was reached in the study of Cl^- desorption from condensed Cl_2.[6]

The O^- kinetic energy distributions (Fig. 3) give information on the dissociation limits of the three O_2^- compound states. The curves at E_i=12 and 13 eV show that the 13-eV compound state dissociates into the lowest two limits and the probability for dissociation into the second lowest limit is larger than that into the first. The E_i=7.7eV curve shows that the 7-eV compound state dissociates only into the lowest limit. The dissociation limits of the 8.5-eV compound state cannot be obtained directly from Fig. 3; however, it can be deduced by the following argument. The 7-eV compound state yields predominantly 1.7-eV (=(7.0-3.65)/2) O^- ions, provided that the momentum transfer to the O_2 lattice is negligible. The retarding potential V_R=-1.8eV is strong enough to discriminate such low-energy ions, and indeed the 7-eV peak disappears in the V_R=-1.8eV curve (see Fig. 1). Similarly, if the 8.5-eV compound state predominantly dissociates into the second lowest limit, the dominant O^- kinetic energy would be 1.5 eV (=(8.5-5.62)/2). The retarding potential V_R=-1.8eV should discriminate such low-energy O^- ions. The presence of the 8.5-eV peak in the V_R=-1.8eV curve (Fig. 1), therefore, indicates that the 8.5-eV compound state predominantly dissociates into the lowest limit.

C. Widths

The widths of the 8.5- and 13-eV features can be estimated from the curves in Figs. 1 and 2. From the O_2/Pt(V_R=-1.5 and -1.8eV) curves in Fig. 1, we estimate FWHMs for the 8.5- and 13-eV features to be 2.3±0.4 and 2.1±0.4 eV, respectively. In these estimates, the energy spread of the electron beam (0.3 eV) has been taken into account. From the 8.5-eV feature in the $O_2^-/(O_2)_n$ curve and the 13-eV feature in the $OH^-/C_6H_{14}/O_2$ curve, we estimate their FWHMs to be 2.2±0.3 and 2.3±0.4 eV, respectively. The energy spreads of the electron beams in these experiments are 0.5 eV (Ref. 7) and 0.3 eV (Ref. 6) respectively. The two estimates (i.e., 2.3 and 2.2 eV for the 8.5-eV feature and 2.1 and 2.3 eV for the 13-eV feature) agree reasonably well.

We can estimate the contribution of a compound state to the O^- yield curve utilizing its FWHM. The shaded area in Fig. 1 shows such a contribution estimated with a FWHM=2.1eV and the electron beam spread=0.3eV for the 13-eV feature. Figure 1 indicates a slowly varying background under the 13-eV feature. This background is due to multiple-electron scattering and is expected to vary slowly. We have already seen the presence of multiple-electron scattering in the O^- kinetic energy distribution (Fig. 3), namely the contributions marked with open triangles. The multiple-electron scattering in Fig. 3 is about 50 % at 13 eV, which agrees with the background contribution (about 50 %) at 13 eV in Fig. 1. This agreement supports the FWHM=2.1eV estimate for the width of the 13-eV compound state. In conclusion, we estimate the widths of the 8.5- and 13-eV features to be 2.2±0.3 and 2.1±0.4 eV, respectively. The width of the 7-eV feature, which is observed in the O^- yield curve of O_2 gas, is 2.0±0.2 (Refs. 3 and 9).

D. Summary

Table I summarizes the observed characteristics of the 7-, 8.5-, and 13-eV compound states. For all three states, the survival rate against autodetachment (i.e., $O_2^- \rightarrow O_2+e^-$) during dissociation into an $O+O^-$ limit must be substantial, because O^- ions from these three compound states are observed. The vertical energies in the table are measured from the O_2 ground state (v=0) to the peaks observed in the ion yield curves. The FWHMs are the widths observed in the ion yield curves. The "1" and "2" in the "Dissociation limit" column stand for the lowest and the second lowest $O+O^-$ dissociation limits. In the following sections, we shall identify these three compound states using their characteristics listed here.

III. THEORETICAL ANALYSES

A. Vertical energies

Tables II, III, and IV list the observed and estimated vertical energies measured from the O_2 ground state to the O_2, O_2^+, and O_2^- valence states, respectively. The valence states are identified by their electronic configurations (EC) and state symmetries except for the three $O_2^+(1\pi_u^{-1})\,{}^2\Pi_u$ states, which have an additional label, I, II, or III. When a valence state mixes strongly with Rydberg states, such as the O_2 ${}^3\Pi_u(1\pi_u^{-1}3\sigma_u)$ valence state with the ${}^3\Pi_u(1\pi_g^{-1}3p\sigma_u)$ Rydberg state, the pure valence state energy is estimated from analyses presented in the literature. All the vertical energies listed in the three tables represent pure valence state energies. The references on which the experimental data or analyses are based are cited in the tables.

In these three tables, estimated (as opposed to observed) vertical energies are enclosed in parentheses. Table V shows how we estimate an unobserved vertical energy from theoretical calculations, using the $O_2^+(1\pi_u^{-1})^2\Pi_u(II)$ state as an example. Although theoretical calculations may not accurately reproduce the absolute energy splittings arising from a given electronic configuration, they usually reproduce the relative energy splittings, as shown in Table V (compare the "Experiment" and "Theory" columns). In other words, when a scale factor is included and optimized such that the scaled energies reproduce the observed splittings as closely as possible, we usually obtain excellent agreement with experiment. Adopting the estimated splitting 4.1 eV for $O_2^+(1\pi_u^{-1})^2\Pi_u(II)$—$O_2^+(1\pi_u^{-1})^4\Pi_u$ and the observed energy 16.70 eV for the $O_2^+(1\pi_u^{-1})^4\Pi_u$ state, we estimate the $O_2^+(1\pi_u^{-1})^2\Pi_u(II)$ state energy to be 20.8 eV. This estimated energy is listed in Table III and enclosed in parentheses. The theoretical calculations utilized are cited in the "Reference" columns. When theoretical calculations are not available, such as for the $2\sigma_g^{-1}$ and $2\sigma_g^{-1}1\pi_g$ cases, we use the relative energies of analogous ECs, such as $3\sigma_g^{-1}$ and $3\sigma_g^{-1}1\pi_g$, for the above examples.

The configuration center (CC) of an electronic configuration (EC) is defined as a weighted average of state energies arising from the EC. Tables II, III, and IV include such CCs, which are calculated from the vertical energies. The averaged vertical excitation energy (AVEE) can be calculated from a pair of CCs. For example, the AVEE for the $1\pi_u \rightarrow 1\pi_g$ excitation can be calculated from the differences of the following three pairs: O_2^+ $1\pi_u^{-1}$ and $1\pi_g^{-1}$, O_2 $1\pi_u^{-1}1\pi_g$ and the GSC (the ground state configuration of O_2), or O_2^- $1\pi_u^{-1}1\pi_g^2$ and $1\pi_g$. Table VI compares the AVEEs calculated from the different pairs of CCs. This comparison clearly shows that the AVEEs are nearly independent of the molecular charge. Assuming this independence, we can often predict the CCs of O_2^- states with an uncertainty of less than 1 eV.

We expect the charge independence in the AVEE's based on the following argument. The CC of an EC specified by a set of electron occupation numbers $\{n_1,n_2,\cdots\}$ is given to a good approximation by

$$E_{CC}(n_1,n_2,\cdots) = A + \Sigma_i B_i n_i + \Sigma_{ij} C_{ij} n_i n_j \ , \qquad (10)$$

where A, B_i, and C_{ij} are independent of occupation numbers. The quadratic coefficients C_{ij} are symmetric with exchange of indexes and approximately satisfy the relation,

$$C_{ij} \approx (C_{ii} + C_{jj})/2 \ . \qquad (11)$$

Further, the diagonal coefficients C_{ii} are approximately proportional to

$$C_{ii} \propto \iint \psi_i(r_1)^2 \,(1/|r_1-r_2|)\, \psi_i(r_2)^2 \, dr_1 dr_2 \ , \qquad (12)$$

where $\Psi_i(r)$ is the i-th molecular orbital (MO). Using Eqs. (10) and (11), we have the AVEE for the 1→2 excitation,

$$E_{ee}(n_1-1,n_2+1,\cdots) - E_{ee}(n_1,n_2,\cdots)$$
$$\approx B_2 - B_1 + (C_{22} - C_{11})\Sigma_i n_i \ . \qquad (13)$$

Expression (13) shows that the AVEE should depend on $\Sigma_i n_i$ or the total charge of a molecule, which is a sum of nuclear charges minus $\Sigma_i n_i$. For homonuclear diatomic molecules, however, we have $C_{ii} \approx C_{jj}$ to a very good approximation among valence MOs i and j, because the Coulomb integral, Eq. (12), is insensitive to the details of the $\Psi_i(r)^2$ distribution, and because $\Psi_i(r)^2$ for valence MOs in a homonuclear diatomic molecule are similar in size and localization. Hence, for a valence excitation of homonuclear diatomic molecules, we should have

$$E_{cc}(n_1-1,n_2+1,\cdots) - E_{cc}(n_1,n_2,\cdots) \approx B_2 - B_1 \ . \qquad (14)$$

This explains the near independence on molecular charge and justifies the use of the AVEEs for predicting other unobserved O_2^- states.

There are several ways to estimate the unobserved vertical energies of the O_2^- compound states. For example, we can estimate the vertical CC of the $3\sigma_g^{-1}1\pi_g^2$ configuration from any of the following three equations,

$$3\sigma_g^{-1}1\pi_g^2 - 1\pi_g \ (0.2 \text{ eV}) = 7.5 \text{ eV} \ , \qquad (15)$$

$$3\sigma_g^{-1}1\pi_g^2 - 1\pi_u^{-1}1\pi_g^2 \ (7.8 \text{ eV}) = 0.6 \text{ eV} \ , \qquad (16)$$

$$3\sigma_g^{-1}1\pi_g^2 - 3\sigma_u \ (10.6 \text{ eV}) = -2.5 \text{ eV} \ , \qquad (17)$$

where the right hand sides of the above equations are the AVEEs for O_2 listed in Table VI. Although we could use the AVEEs for O_2^+ instead of O_2, we prefer the O_2 data to the O_2^+ data because the total charge difference between O_2 and O_2^- is smaller than that between O_2^+ and O_2^-. These equations give the $3\sigma_g^{-1}1\pi_g^2$ energy as 7.7, 8.4, and 8.1 eV, respectively. Averaging these three, we estimate the $3\sigma_g^{-1}1\pi_g^2$ energy to be 8.1 eV with a probable uncertainty of ±0.9 eV. This and similarly estimated vertical energies for the lower-lying O_2^- valence states are listed in Table VII. The listed ECs are the lowest 7; the next lowest EC is located around 24 eV.

We have excluded O_2^- Rydberg states, that is the $v^{-1}Ryd^2$ states, from our considerations for the 8.5- and 13-eV compound states, because Rydberg states are not observed in the solid phase and probably do not exist in the solid. Even if the O_2^- Rydberg states do exist in the solid, they most likely do not dissociate into an $O+O^-$ limit. In any event, we find that some of our estimated O_2^- valence states agree nicely with the 8.5- and 13-eV features observed in the O^- yields. In the following sections, we restrict ourselves to the O_2^- valence states.

B. Properties of the O_2^- valence states

Table VII summarizes the properties of the lower-lying O_2^- valence states. We explain each property in the following subsections.

1. Electron attachment

According to the selection rules described in Sec. I, we can classify electron attachments into three categories: allowed with one-electron excitation (A(1)), allowed with two-electron excitations (A(2)), and forbidden (F). The attachment probability of A(1) excitations is generally much higher than that of A(2). The possible lower-energy-electron attachments from the O_2 ground state ($^3\Sigma_g^-$) are classified as above and listed in Table VII. Although the formation of the $^2\Delta_u(3\sigma_u)$ state appears to be A(1), it is not A(1) but A(2) because the $^2\Delta_u(3\sigma_u)$ state arises from the $1\pi_g^2(^1\Delta_g)3\sigma_u$ configuration but the initial state has the $1\pi_g^2(^3\Sigma_g^-)\varepsilon\delta_u$ configuration. Here, $\varepsilon\delta_u$ represents an incoming electron orbital of kinetic energy ε and symmetry δ_u. All forbidden attachments in the table are due to the σ^- selection rule. These $\Sigma^- \nleftrightarrow \Sigma^+$ forbidden attachments are expected to relax in the solid phase; the analogous $\Sigma^- \nleftrightarrow \Sigma^+$ forbidden photoabsorption processes are indeed observed in solid O_2.[2]

2. Electron detachment

Figure 5 illustrates a dissociative attachment process accompanied with autodetachment or autoionization, also called electron detachment. The O_2^- state, which is formed by electron impact of energy E, autoionizes into an O_2 state, when $W^-(R) > W(R)$ or $R_t < R < R_c$. Here, $W^-(R)$ and $W(R)$ are the potential energy curves of the O_2^- and O_2 states, R_t is the turning point of the $W^-(R)$ at the energy E, and R_c is the crossing point of the two potential curves (see Fig. 5). In order to dissociate into an O+O$^-$ limit, the O_2^- state must survive against the above-mentioned autoionization. According to Bardsley et al.,[26] the dissociative attachment cross section $\sigma_{DA}(E)$ for the above process is given approximately by

$$\sigma_{DA}(E) = \sigma_{AT}(E)\ \exp\{-\int_{R_s}^{R_c} dR\ \Gamma(R)/\hbar v(R)\}\ , \qquad (18)$$

where $\sigma_{AT}(E)$ is the cross section for formation of the O_2^- state; $\Gamma(R)$ is the width of the O_2^- state with respect to the autoionization; and $v(R)$ is the relative velocity of the nuclei. The exponential factor in Eq. (18) represents the probability that the O_2^- state survives against the autoionization.

$\Gamma(R)$ for one-electron processes, such as

$$O_2^-(1\pi_u^{-1}1\pi_g^{2})\,^2\Pi_u \rightarrow O_2(1\pi_u^{-1}1\pi_g)\,^3\Sigma_u^+ + e^-\ , \qquad (19)$$

is governed by the kinetic energy of the outgoing electron ($\Delta W(R)=W^-(R)-W(R)$) and the asymptotic angular momentum ℓ of the outgoing electron through the centrifugal barrier. For small ΔW, Γ is proportional to

$$\Gamma \propto \Delta W^{\ell+1/2}\ , \qquad (20)$$

for a one-electron process, and, in general, Γ increases monotonicly with ΔW.[27] For two-electron processes, on the other hand, Γ is a slowly varying function of ΔW and is orders of magnitude smaller than that for one-electron processes, except for the $\Delta W \ll 1$ case. Since the survival factor depends exponentially on Γ [Eq. (18)], the survival factor for one-electron processes is several orders of magnitude smaller than that for two-electron processes except again for the ΔW << 1 case.

The magnitude for autoionization via one-electron processes can be characterized by a pair of parameters, $\Delta W(R_e)$ and ΔR_{ce} ($=R_c-R_e$), where R_e is the equilibrium internuclear distance for the O_2 ground state. Both parameters are referred to R_e because the initial O_2^- state is formed with the highest probability at $R=R_e$ according to the Franck-Condon principle. The larger the $\Delta W(R_e)$ and ΔR_{ce}, the smaller the σ_{DA} (or O^- yield). These $\Delta W(R_e)$ and ΔR_{ce} parameters are listed in Table VII.

There are two types of states in Table VII: those which autoionize by detaching the $1\pi_g$ electron and those by detaching the $3\sigma_u$ electron. The states in the former group have much smaller $\Delta W(R_e)$ and ΔR_{ce} than those in the latter group. The $O_2^-(3\sigma_u)\,^4\Sigma_u^-$ state, one of the latter group, dominates the vibrational excitation spectra.[24] This state, however, does not appear in the O^- yield curve,[9] indicating that the survival rate of this state is negligibly small. Other states in the latter group also should have negligible survival rates, since they have larger $\Delta W(r_e)$ and ΔR_{ce} than the $O_2^-(3\sigma_u)\,^4\Sigma_u^-$ state. In short, all states which autoionize by detaching the $3\sigma_u$ electron cannot appear in the O^- yield curve. On the other hand, the $O_2^-(1\pi_u^{-1}1\pi_g^{2})\,^2\Pi_u$ state, one of the former group, has been observed in the O^- yield curve,[9] indicating that the survival rate of this state is substantial. Since other states in the former group have smaller $\Delta W(R_e)$ and ΔR_{ce} than this state, they should have even larger survival rates. In other words, all states which autoionize by detaching the $1\pi_g$ electron, except for the O_2^- $(1\pi_g)^2\Pi_g$ state, can produce O^- ions if they are formed. The O_2^- $(1\pi_g)^2\Pi_g$ state cannot produce O^- ions, because its vertical energy (0.21 eV) is much lower than the lowest $O+O^-$ dissociation limit (3.65 EV). In conclusion, the survival rate analyses indicate that only three O_2^- states, $^2\Pi_u(1\pi_u^{-1}1\pi_g^2)$, $^2\Sigma_g^+(3\sigma_g^{-1}1\pi_g^2)$, and $^2\Sigma_u^+(2\sigma_u^{-1}1\pi_g^2)$, can produce ample O^- ions.

Figure 6 schematically shows $\sigma_{DA}(E)$, $\sigma_{AT}(E)$, and SF(E) (survival factor) as a function of the incident electron energy E. $\sigma_{AT}(E)$ has a peak at $E=W^-(R_e)$ because of the Franck-Condon principle. SF(E) is unity below $E=W^-(R_c)$, since $\Gamma=0$ in this region, and decreases monotonicly with increasing E, since the integrand of the survival factor is always positive and the lower integration limit (R_x) decreases with increasing E [see Eq. (18)]. Since $\sigma_{DA}(E)=\sigma_{AT}(E)SF(E)$, the peak position of $\sigma_{DA}(E)$ should be shifted to lower energy relative to that of $\sigma_{AT}(E)$. This means that a peak position observed in the O^- yield (a σ_{DA} peak) should be lower than the corresponding vertical energy (the σ_{AT} peak). Indeed, the O^- yield peak observed at 6.7 eV, which is due to the $O_2^-(1\pi_u^{-1}1\pi_g^2)^2\Pi_u$ resonance, is lower than the vertical energy 7.8 eV by 1.1 eV.[23] For the $O_2^-(3\sigma_g^{-1}1\pi_g^2)^2\Sigma_g^+$ and $O_2^-(2\sigma_u^{-1}1\pi_g^2)^2\Sigma_u^+$ resonances, we expect smaller shifts (< 0.3 eV) than for the $O_2^-(1\pi_u^{-1}1\pi_g^2)^2\Pi_u$ resonance, because the former two states have smaller $\Delta W(R_e)$ and ΔR_{ec} parameters than the latter state.

3. Franck-Condon widths

The width of the repulsive *O_2^- compound* state is predominantly governed by the Franck-Condon overlap integral between the *$v=0$* vibrational wavefunction of the O_2 ground state, $\Psi_0(R)$, and the vibrational wavefunction of the repulsive O_2^- compound state. In the reflection approximation,[28,29] the repulsive wavefunction can be replaced by a *δ function* which differs *from* zero only at the classical turning point. The results obtained with this replacement, deviate only slightly from those obtained with accurate wavefunctions.[30] With this approximation, the Franck-Condon width (FCW) of the repulsive O_2^- compound states can be given,

$$\mathrm{FCW} = \Delta R(v=0) \times |dW^-(R)/dR|_{R=R_e}, \tag{21}$$

where $\Delta R(v=0)$ is the FWHM of $\Psi_0(R)^2$, because $W^-(R)$ of a repulsive state is nearly linear over the Franck-Condon region.

The FCWs in Table VII are estimated from theoretical calculations in the literature, except for the FCW of the $^2\Pi_u(1\pi_u^{-1}1\pi_g^2)$ state. The FCW of this state is calculated from the experimental slope determined by O'Malley.[23] The slopes (i.e., $dW^-(R)/dR$ at $R=R_e$) for the $^2\Pi_g(1\pi_g)$, $^4\Sigma_u^-(3\sigma_u)$, and $^2\Sigma_u^-(3\sigma_u)$ states are calculated from the MCSCF results[28] by quadratic curve fittings. The data in parentheses are estimated by assuming empirical relations such as

$$\begin{aligned}&\mathrm{Slope}(3\sigma_g^{-1}1\pi_g^2) - \mathrm{Slope}(1\pi_u^{-1}1\pi_g^2)\\ &\qquad \approx \mathrm{Slope}(3\sigma_g^{-1}1\pi_g) - \mathrm{Slope}(1\pi_u^{-1}1\pi_g)\ . \end{aligned}\tag{22}$$

The error ranges for the FCWs (2.4 and 2.2 eV) of the $^2\Sigma_g^+(3\sigma_g^{-1}1\pi_g^2)$ and $^2\Sigma_u^+(2\sigma_u^{-1}1\pi_g^2)$ states may be around ±0.4 eV.

There are two experiments which reflect the FCWs. First, the vibrational excitation cross section for $v=1-4$ show a single peak with FWHM of 5.0 eV, which has been attributed to the $O_2^-(3\sigma_u)\,^4\Sigma_u^-$ resonance.[24] The FWHM (5.0 eV) of the vibrational cross section should be larger than that (4.3 eV) of the electron attachment, supporting our estimate of 4.3 eV. Second, the O^- yield due to the $O_2^-(1\pi_u^{-1}1\pi_g^2)\,^2\Pi_u$ resonance has a FWHM of 2.0 eV.[3] The difference between the FWHM (2.0 eV) of the O^- yield and the FCW (3.0 eV) of this compound state is caused by a sizable autodetachment rate (see Fig. 6).[23] Since autodetachment from the $O_2^-(3\sigma_g^{-1}1\pi_g^2)\,^2\Sigma_g^+$ and $O_2^-(2\sigma_u^{-1}1\pi_g^2)\,^2\Sigma_u^+$ compound states should be much smaller than that from the $O_2^-(1\pi_u^{-1}1\pi_g^2)\,^2\Pi_u$ state, the FWHMs of these two compound states in the O^- yield curve should be close to their FCWs.

4. Dissociation limit

The dissociation limits of the lower-lying O_2^- valence states can be determined by the non-crossing rule. The molecular states resulting from the two lowest dissociation limits of $O+O^-$, known from Wigner-Witmer rules,[31] are listed in Table VIII. According to the non-crossing rule, these molecular states must be connected to the O_2^- valence states with the same symmetry without crossing each other. This implies, for example, that the lowest $^2\Sigma_u^+$ valence state must be connected to the lowest limit and the second lowest $^2\Sigma_u^+$ valence state to the second lowest limit. Another example, both the lowest two $^2\Pi_g$ valence states must be connected to the lowest limit and the lowest $^2\Phi_u$ valence state to the second lowest limit. Dissociation limits determined as above are listed in Table VII, where "1" and "2" denote the lowest and the second lowest dissociation limits respectively.

Figure 7 shows schematically the potential curves for some of the O_2^- valence states. These curves are drawn based on the data in Table VII (such as the vertical energy, FCW, and dissociation limit) and two theoretical calculations,[32,33] which were carried out only for large internuclear distances (R > 1.6 Å). The apparent avoided curve crossing between the two $^2\Sigma_g^+$ curves is predicted by both calculations. This curve crossing suggests that the $^2\Sigma_g^+$(I) state formed at the Franck-Condon region may end up with the second lowest $O+O^-$ limit.

IV. IDENTIFICATION OF THE O_2^- COMPOUND STATES

Comparing Tables I and VII, we identify the 7-, 8.5, and 13-eV O_2^- compound states to arise from the $^2\Pi_u(1\pi_u^{-1}1\pi_g^2)$, $^2\Sigma_g^+(3\sigma_g^{-1}1\pi_g^2)$, and $^2\Sigma_u^+(2\sigma_u^{-1}1\pi_g^2)$ states, respectively. Almost every aspect (vertical energy, electron attachment probability in the gas phase, survival rate against autodetachment, Franck-Condon broadening, and dissociation limit) supports and confirms these identifications. Moreover, we can exclude alternative identifications: We can exclude the $O_2^-(1\pi_g)\,^2\Pi_g$ state, because its vertical energy is much lower than the lowest $O+O^-$ limit. The O_2^- states arising from the $3\sigma_u$, $1\pi_u^{-1}1\pi_g3\sigma_u$, and $3\sigma_g^{-1}1\pi_g3\sigma_u$ configurations have survival rates which are too small to yield O^- ions and FCWs which are too large for the observed line widths. Furthermore, states from the last two ECs have vertical energies which are too high to be any of the three features. Hence, we conclude that the 8.5- and 13-eV features are due to the $O_2^-(3\sigma_g^{-1}1\pi_g^2)\,^2\Sigma_g^+$ and $O_2^-(2\sigma_u^{-1}1\pi_g^2)\,^2\Sigma_u^+$ compound states. This identification implies that the absence of these features in the gas phase is due to the σ^- selection rule.

V. PREVIOUS INTERPRETATIONS

The 8.5- and 13-eV features have been interpreted previously. Xiang and Lichtman,[6] who reported the O^- yield curve from O_2/W (Fig. 1), attributed the 13 eV peak to the $O_2^-(1\pi_u^{-1}1\pi_g^2)\,^2\Pi_u$ state, or the "7-eV" state, which was regarded as shifted because of a substrate effect. They overlooked a weak 8.5-eV feature in their spectrum. Sanche and co-workers,[5,6] who reported the three O^- yield curves from O_2/Pt (Fig. 1) and the OH^-–$C_6H_{14}/O_2/Pt$ spectrum in Fig. 2, assigned the $O_2^-(3\sigma_g^{-1}1\pi_g^2)\,^2\Sigma_g^+$ state (that is, the "8.5-eV" state) to the 13-eV feature. Further, the absence of the 13-eV feature in the gas-phase spectrum was attributed to the angular dependence rule given by Dunn,[26] rather than to the σ^- selection rule.[1] Märk _et al._,[7] who reported the $O_2\cdot O^-$ and O_2^- yields from $(O_2)_n$ clusters (Fig. 2), attributed both the 7-eV and 8.5-eV features to the $O_2^-(1\pi_u^{-1}1\pi_g^2)\,^2\Pi_u$ state. Our analyses in this work do not support any of the above interpretations.

Acknowledgement

We greatly acknowledge fruitful cooperation with Dr. L. Sanche's group. This work was partially supported by the Office of Naval Research.

References

[1] H. Sambe and D. E. Ramaker, Chem. Phys. Lett. 139, 386 (1987).

[2] A. M. Bass and H. P. Broida, J. Mol. Spectrosc. 12, 221 (1964).

[3] D. Rapp and D. D. Briglia, J. Chem. Phys. 43, 1480 (1965).

[4] L. Z. Xiang and D. Lichtman, Surf. Sci. 114, 287 (1982).

[5] R. Azria, L. Parenteau, and L. Sanche, Phys. Rev. Lett. 59, 638 (1987).

[6] L. Sanche and L. Parenteau, Phys. Rev. Lett. 59, 136 (1987).

[7] T. D. Märk, K. Leiter, W. Ritter, and A. Stamatovic, Phys. Rev. Lett. 55, 2559 (1985).

[8] R. Azria, L. Parenteau, and L. Sanche, J. Chem. Phys. 87, 2292 (1987).

[9] G. J. Schulz, Rev. Mod. Phys. 45, 423 (1973).

[10] K. P. Huber and G. Herzberg, Molecular Spectra and Molecular Structure --Constants of Diatomic Molecules (Van Nostrand Reinhold Comp., New York, 1979).

[11] K. Wakiya, J. Phys. B 11, 3931 (1978).

[12] R. P. Saxon and B. Liu, J. Chem. Phys. 67, 5432 (1977).

[13] D. Spence, J. Chem. Phys. 74, 3898 (1981).

[14] R. J. Buenker, S. D. Peyerimhoff, and M. Perić, Chem. Phys. Lett. 42, 383 (1976); L. C. Lee, T. G. Slanger, G. Black, and R. L. Sharpless, J. Chem. Phys. 67, 5602 (1977).

[15] H.-J. Hinz, in Proceedings of the 4th International Conference on Vacuum Ultraviolet Radiation Physics, Hamburg, 1974, edited by E. E. Koch (Pergamon, Oxford, 1974), p. 176.

[16] J. S. Lee, J. Chem. Phys. 67, 3998 (1977).

[17] O. Edqvist, E. Lindholm, L. E. Selin, and L. Åsbrink, Phys. Scripta. 1, 25 (1970).

[18] N. Jonathan et al., J. Chem. Soc. Faraday Trans. II 70, 1810 (1974).

[19] R. N. Dixon and S. E. Hull, Chem. Phys. Lett. 3, 367 (1969).

[20] M. S. Banna and D. A. Shirley, J. Electron Spectrosc. Related Phenomena 8, 255 (1976).

[21] K. Siegbahn *et al.*, *ESCA Applied to Free Molecules* (North-Holland, Amsterdam, 1969).

[22] R. J. Celotta *et al.*, Phys. Rev. A 6, 631 (1972).

[23] T. F. O'Malley, Phys. Rev. 155, 59 (1967).

[24] S. F. Wong, M. J. W. Boness, and G. J. Schulz, Phys. Rev. Lett. 31, 969 (1973).

[25] G. Das, A. C. Wahl, W. T. Zemke, and W. C. Stwalley, J. Chem. Phys. 68, 4252 (1978).

[26] J. N. Bardsley, A. Herzenberg, and F. Mandl, Proc. Phys. Soc. London 89, 321 (1966).

[27] D. T. Birtwistle and A. Herzenberg, J. Phys. B 4, 53 (1971); J. M. Blatt and V. F. Weisskopf, *Theoretical Nuclear Physics* (John Wiley & Sons, New York, 1952), p. 390, equation (7.15).

[28] J. G. Winans and E. C. G. Stueckelberg, Proc. Nat. Acad. Sci. USA 14, 867 (1928).

[29] G. Herzberg, *Molecular Spectra and Molecular Structure* (D. Van Nostrand Comp., New York, 1950), Vol. 1.

[30] A. S. Coolidge, H. M. James, and R. D. Present, J. Chem. Phys. 4, 193 (1936).

[31] E. Wigner and E. E. Witmer, Z. Phys. 51, 859 (1928).

[32] M. Krauss *et al.*, Phys. Rev. A 7, 69 (1973).

[33] H. H. Michels and F. E. Harris, in Seventh International Conference on the Physics of Electronic and Atomic Collisions, Amsterdam, 1971 (North-Holland, Amsterdam, 1971), Vol. II, p. 1170.

[34] G. H. Dunn, Phys. Rev. Lett. 8, 62 (1962).

TABLE I. Summary of experimental findings on the 7-, 8.5-, and 13-eV O_2^- compound states.

Name	Vertical energy (eV)[a]	O^- yield from O_2 gas	Survival rate[b]	FWHM (eV)[c]	Dissociation limit
"7-eV"	6.7	large	large	2.0±0.1	"1"[d]
"8.5-eV"	8 - 9	negligible	large	2.7±0.3	"1"
"13-eV"	13	negligible	large	2.4±0.3	"2"

[a] From the O_2 ground state to peak positions in the O^- yield curves.

[b] Survival rate against autodetachment.

[c] Widths observed in the ion yield curves.

[d] "1" and "2" denote the lowest and the second lowest $O+O^-$ dissociation limits.

TABLE II. Observed and estimated vertical energies (eV) of the lower-lying O_2 states. Estimated energies are enclosed in parentheses.

Electronic configuration	Configuration center (eV)	State symmetry	Vertical energy (eV)	Reference
Ground state	0.60	$^3\Sigma_g^-$	0.00	10
		$^1\Delta_g$	0.98	10
		$^1\Sigma_g^+$	1.63	10
$1\pi_u^{-1}1\pi_g$	7.5	$^1\Sigma_u^-$	5.8	10, 11
		$^3\Delta_u$	6.0	10, 11
		$^3\Sigma_u^+$	6.1	10, 11
		$^3\Sigma_u^-$	8.5	11
		$^1\Delta_u$	(10.8)	12
		$^1\Sigma_u^+$	(12.6)	12
$3\sigma_g^{-1}1\pi_g$	8.1	$^3\Pi_g$	7.7	13
		$^1\Pi_g$	(9.2)	12
$1\pi_g^{-1}3\sigma_u$	10.6	$^3\Pi_u$	10.2	14
		$^1\Pi_u$	(11.9)	12
$2\sigma_u^{-1}1\pi_g$	14.3	$^3\Pi_u$	14.2	15
		$^1\Pi_u$	(14.6)	12
$2\sigma_g^{-1}1\pi_g$	28.9 ± 1.0	$^3\Pi_g$	28.5 ± 1.0	16
		$^1\Pi_g$	(30.0)[a]	--

[a] Estimated from the splitting energies of the $3\sigma_g^{-1}1\pi_g$ states.

TABLE III. Observed and estimated vertical energies (eV) of the lower-lying O_2^+ states. Estimated energies are enclosed in parentheses.

Electronic configuration	Configuration center (eV)	State symmetry	Vertical energy (eV)	Reference
$1\pi_g^{-1}$	12.31	$^2\Pi_g$	12.31	17
$1\pi_u^{-1}$	19.2	$^4\Pi_u$	16.70	17
		$^2\Pi_u$(I)	17.73	17
		$^2\Phi_u$	19.1	18
		$^2\Pi_u$(II)	(20.8)	19
		$^2\Pi_u$(III)	24.0	17
$3\sigma_g^{-1}$	19.6	$^4\Sigma_g^-$	18.17	17
		$^2\Delta_g$	19.90	18
		$^2\Sigma_g^-$	20.43	17
		$^2\Sigma_g^+$	(20.8)	18
$2\sigma_u^{-1}$	25.9	$^4\Sigma_u^-$	24.58	17
		$^2\Delta_u$	(26.0)	18
		$^2\Sigma_u^+$	(26.8)	18
		$^2\Sigma_u^-$	27.3	20
$2\sigma_g^{-1}$	40.0	$^4\Sigma_g^-$	38.8	21[a]
		$^2\Delta_g$	(40.3)[b]	--
		$^2\Sigma_g^-$	40.8	21[a]
		$^2\Sigma_g^+$	(41.1)[b]	--

[a] The energy scale is shifted by 0.8 eV to make the first-peak energy position agree with the accurate energy 12.3 eV.

[b] Estimated from the splitting energies of the $3\sigma_g^{-1}$ states.

TABLE IV. Observed and estimated vertical energies (eV) of the lower-lying O_2^- states. Estimated energies are enclosed in parentheses.

Electronic configuration	Configuration center (eV)	State symmetry	Vertical energy (eV)	Reference
$1\pi_g$	0.21	$^2\Pi_g$	0.21	22
$1\pi_u^{-1}1\pi_g^2$	7.8 ± 0.2	$^2\Pi_u$	7.8 ± 0.2	23[a]
$3\sigma_u$	10.6 ± 0.3	$^4\Sigma_u^-$	9.5 ± 0.3	24
		$^2\Delta_u$	(10.7)[b]	--
		$^2\Sigma_u^+$	(11.5)[b]	--
		$^2\Sigma_u^-$	(11.9)	25[c]

[a] The uncertainty indicates the sensitivity of the fitting and thus does not reflect absolute errors.

[b] Estimated from the splitting energies of the $2\sigma_u^{-1}$ states.

[c] Estimated using the $^4\Sigma_u^-$-$^2\Sigma_u^-$ energy difference calculated by MCSCF with 65 configurations.

TABLE V. Energy splittings (eV) of the $O_2^+(1\pi_u^{-1})$ states. The scaled energies are obtained from the unscaled energies by multiplying with a constant factor. This factor is chosen so that the scaled energies reproduce experimental energy splittings as well as possible.

State	Experiment	Theory	
		Scaled	Unscaled
$^4\Pi_u$	0.0	0.0	0.0
$^2\Pi_u$(I)	1.0	1.1	0.9
$^2\Phi_u$	2.4	2.4	2.0
$^2\Pi_u$(II)	---	4.1	3.4
$^2\Pi_u$(III)	7.3	7.3	6.1

TABLE VI. Comparison of averaged vertical excitaion energies (eV).

Excitation	O_2^+	O_2	O_2^-
$1\pi_u \rightarrow 1\pi_g$	6.9 $(1\pi_u^{-1}-1\pi_g^{-1})$	6.9 $(1\pi_u^{-1}1\pi_g$-GSC$)$	7.6 ± 0.2 $(1\pi_u^{-1}1\pi_g^{2}-1\pi_g)$
$3\sigma_g \rightarrow 1\pi_g$	7.3 $(3\sigma_g^{-1}-1\pi_g^{-1})$	7.5 $(3\sigma_g^{-1}1\pi_g$-GSC$)$	-----
$1\pi_g \rightarrow 3\sigma_u$	-----	10.0 $(1\pi_g^{-1}3\sigma_u$-GSC$)$	10.4 ± 0.3 $(3\sigma_u-1\pi_g)$
$2\sigma_u \rightarrow 1\pi_g$	13.6 $(2\sigma_u^{-1}-1\pi_g^{-1})$	13.7 $(2\sigma_u^{-1}1\pi_g$-GSC$)$	-----
$2\sigma_g \rightarrow 1\pi_g$	27.7 $(2\sigma_g^{-1}-1\pi_g^{-1})$	28. $(2\sigma_g^{-1}1\pi_g$-GSC$)$	-----

TABLE VII. Properties of the lower-lying O_2^- valence states.

Electronic configuration	Symmetry	Vertical energy (eV)	Electron attachment	$\Delta W(R_e)$ (eV)	ΔR_{ee} (Å)	Width (eV)	Dissociation limit
$1\pi_g$	$^2\Pi_g$	0.21	A(1)	0.31	0.04	1.2	1
$1\pi_u^{-1}1\pi_g^2$	$^2\Pi_u$	7.8 ± 0.2	A(2)	1.8	0.18	3.0	1
$3\sigma_g^{-1}1\pi_g^2$	$^2\Sigma_g^+$	8.1 ± 0.9	F	(0.4)	(0.04)	(2.4)	1
$2\sigma_u^{-1}1\pi_g^2$	$^2\Sigma_u^+$	14.3 ± 0.9	F	(0.1)	(0.01)	(2.2)	2
$3\sigma_u$	$^4\Sigma_u^-$	9.5 ± 0.3	A(1)	9.6	0.39	4.3	1
	$^2\Delta_u$	10.7 ± 0.5	A(2)	9.8	0.39	(4.4)	1
	$^2\Sigma_u^+$	11.5 ± 0.5	F	10.0	0.40	(4.4)	1
	$^2\Sigma_u^-$	11.9 ± 0.4	A(1)	12.0	0.59	4.5	1
$1\pi_u^{-1}1\pi_g3\sigma_u$	$^4\Sigma_g^+$	17.5 ± 1.0	F	(10.0)	(0.4)	(6.3)	1
	$^4\Sigma_g^-$		A(2)				1
	$^4\Delta_g$		A(2)				1
	$^2\Sigma_g^+(2)$		F				2
	$^2\Sigma_g^-(2)$		A(2)				1
	$^2\Delta_g(2)$		A(2)				1 & 2
$3\sigma_g^{-1}1\pi_g3\sigma_u$	$^4\Pi_u$	18.1 ± 1.0	A(2)	(10.0)	(0.4)	(5.7)	1
	$^2\Pi_u(2)$		A(2)				1 & 2

TABLE VIII. Dissociation limits of the O_2^- valence states which have the lower energies in the Franck-Condon region.

Dissociation limit	Molecular states belonging to the dissociation limit	O_2^- valence state		
		Symmetry	Electronic configuration	Vertical energy (eV)
$O^-(^2P_u) + O(^3P_g)$	$^2\Sigma_u^+$, $^2\Sigma_g^+$, $^4\Sigma_u^+$, $^4\Sigma_g^+$, $^2\Sigma_u^-(2)$, $^2\Sigma_g^-(2)$, $^4\Sigma_u^-(2)$, $^4\Sigma_g^-(2)$, $^2\Pi_u(2)$, $^2\Pi_g(2)$, $^4\Pi_u(2)$, $^4\Pi_g(2)$, $^2\Delta_u$, $^2\Delta_g$, $^4\Delta_u$, $^4\Delta_g$	$^2\Pi_g(I)$	$1\pi_g$	0.2
		$^2\Pi_u(I)$	$1\pi_u^{-1}1\pi_g^2$	7.8
		$^2\Sigma_g^+(I)$	$3\sigma_g^{-1}1\pi_g^2$	8.1
		$^4\Sigma_u^-(I)$	$3\sigma_u$	9.5
		$^2\Delta_u(I)$	$3\sigma_u$	10.7
		$^2\Sigma_u^+(I)$	$3\sigma_u$	11.5
		$^2\Sigma_u^-(I)$	$3\sigma_u$	11.9
$O^-(^2P_u) + O(^1D_g)$	$^2\Sigma_u^+(2)$, $^2\Sigma_g^+(2)$, $^2\Sigma_u^-$, $^2\Sigma_g^-$, $^2\Phi_u$, $^2\Phi_g$, $^2\Pi_u(3)$, $^2\Pi_g(3)$, $^2\Delta_u(2)$, $^2\Delta_g(2)$	$^2\Sigma_u^+(II)$	$2\sigma_u^{-1}1\pi_g^2$	14.3
		$^2\Sigma_g^+(II)$	$1\pi_u^{-1}1\pi_g3\sigma_u$	17

Figure captions

FIG. 1. Previously reported electron stimulated O^- desorption yields from O_2/W (Ref. 4), O_2/Pt (Refs. 5 and 6), and O_2 gas (Ref. 3) are plotted as a function of the incident electron energy. V_R denotes the retarding potential applied to the outgoing O^- ions. The shaded area shows our estimated contribution due to the direct process. The vertical dot-dash lines indicate the probable peak positions of the involved O_2^- compound states.

FIG. 2. Previously reported electron stimulated negative ion (O^-, $O_2 \cdot O^-$, O_2^-, or OH^-) desorption yields from O_2 gas (Ref. 3), $(O_2)_n$ clusters (Ref. 7), or C_4H_{14}/O_2/Pt (Ref. 6). The negative ion yields are plotted as a function of the incident *electron energy*. The vertical dot-dash lines indicate the probable peak positions of the involved O_2^- compound states.

FIG. 3. Kinetic energy distributions of the O^- ions from O_2(3ML)/Pt (Ref. 5), which are measured at various incident electron energies, E_i=5.7, 7.7, 12, and 13 eV. The ion energy is referred to the maximum in the distribution with E_i=5.7 eV. Symbols (*closed and open circles and* open triangles) indicate three different contributions. The horizontal bar indicates the possible range of peak position for each contribution.

FIG. 4. The peak positions of the three contributions shown in Fig. 3 are plotted as a function of the incident electron

energy, E_i. The broken straight lines indicate E_{r-i} given by Eq. (4). The E_d values denote the possible $O+O^-$ dissociation limits.

FIG. 5. Schematic potential-energy curves illustrating a dissociative attachment process accompanied with autodetachment. E is the energy of the incident electron. R_t is the turning point of potential curve $W^-(R)$ at the energy E, and R_c is the crossing point of the two potential curves, $W^-(R)$ and $W(R)$.

FIG. 6. Schematic diagram illustrating the two effects: the shift of the $\sigma_{DA}(E)$ peak position relative to the $\sigma_{AT}(E)$ peak and the smaller $\sigma_{DA}(E)$ width in comparison with the $\sigma_{AT}(E)$ width.

FIG. 7. Semi-quantitative potential energy curves, which are based on the data in Table VII and the theoretical calculations of Refs. 32 and 33.

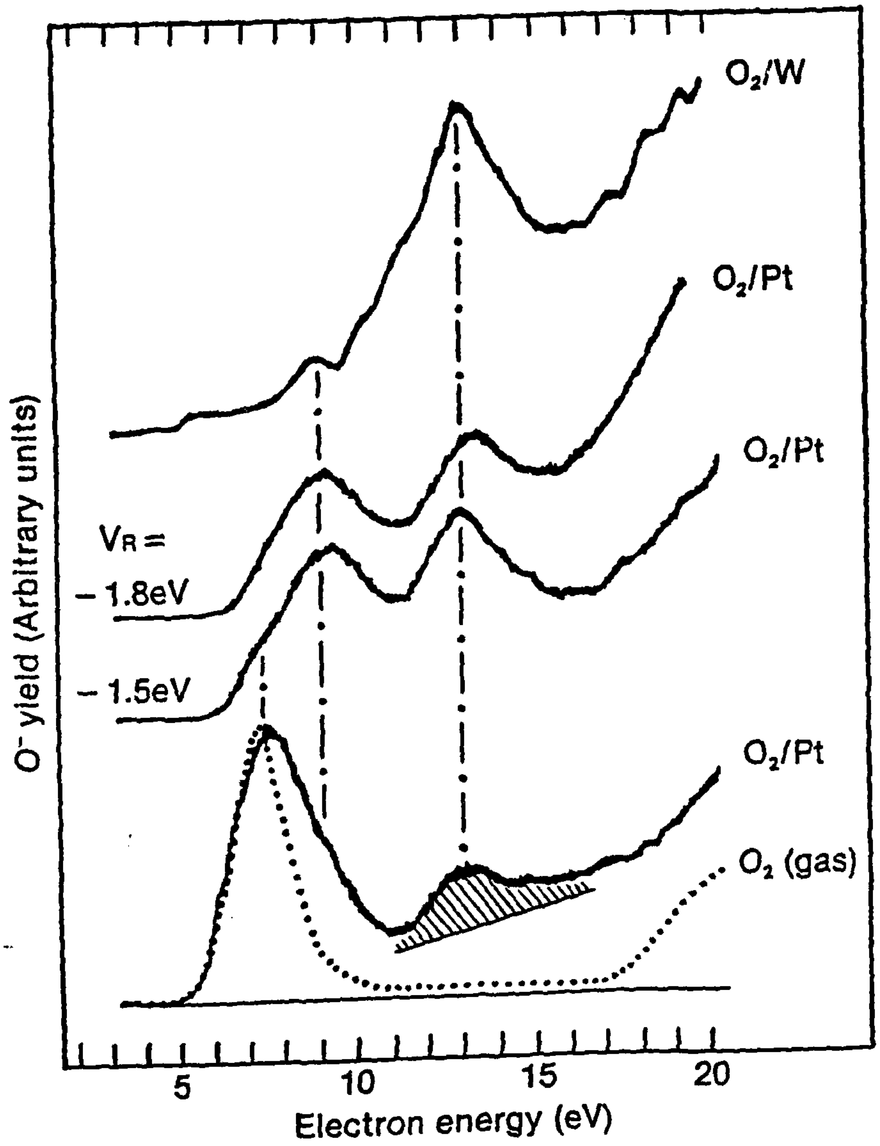

O_2/W
O_2/Pt
O_2/Pt
O_2/Pt
O_2 (gas)
V_R =
− 1.8eV
− 1.5eV
O^- yield (Arbitrary units)
5
10
15
20
Electron energy (eV)

FIG. 1

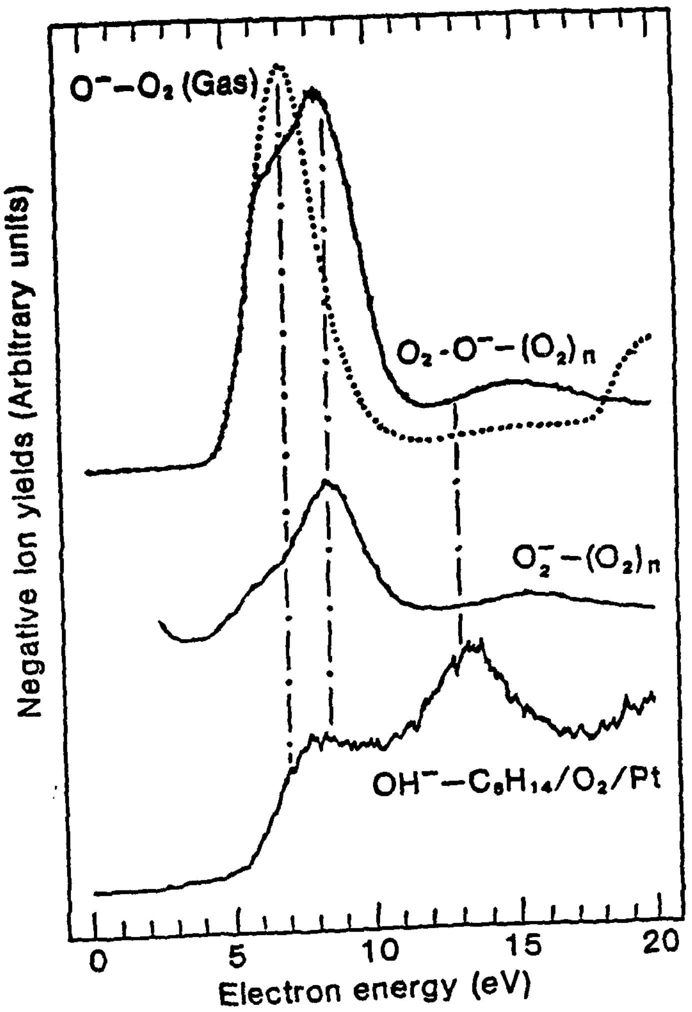
O⁻–O₂ (Gas)
O₂·O⁻–(O₂)n
O₂⁻–(O₂)n
OH⁻–C₆H₁₄/O₂/Pt
Negative ion yields (Arbitrary units)
0
5
10
15
20
Electron energy (eV)

FIG. 2

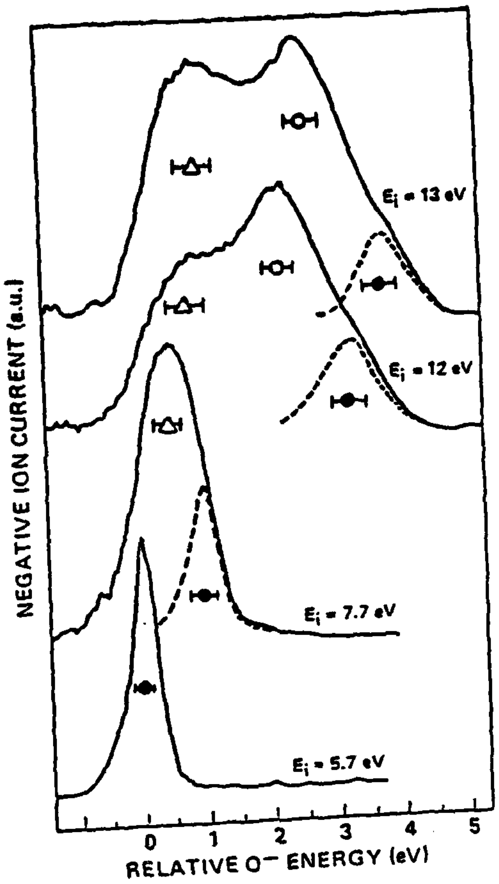
NEGATIVE ION CURRENT (a.u.)
RELATIVE O⁻ ENERGY (eV)
0
1
2
3
4
5
Eᵢ = 13 eV
Eᵢ = 12 eV
Eᵢ = 7.7 eV
Eᵢ = 5.7 eV

FIG. 3

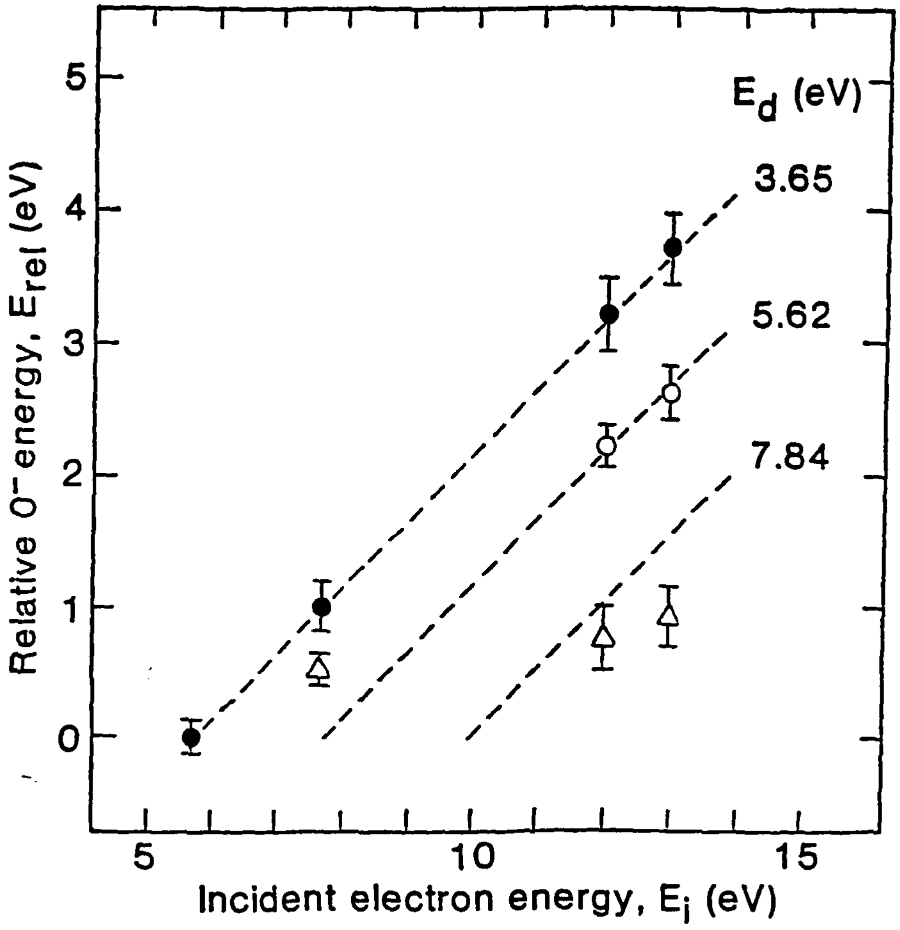
Relative O⁻ energy, E_rel (eV)
Incident electron energy, E_i (eV)
E_d (eV)
3.65
5.62
7.84
0
1
2
3
4
5
5
10
15

FIG. 4

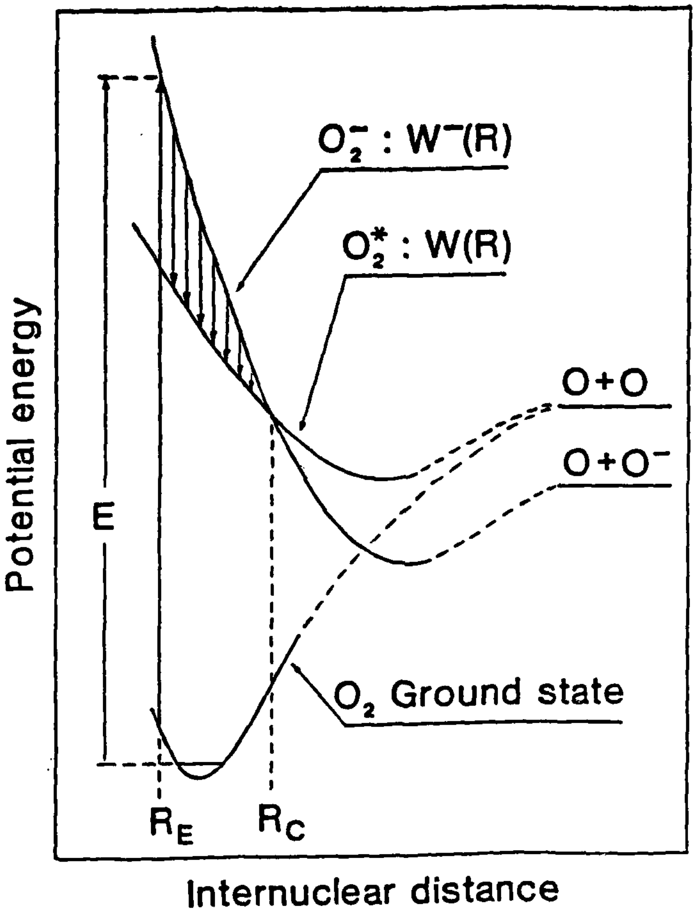
O_2^- : $W^-(R)$
O_2^* : $W(R)$
O+O
O+O$^-$
E
O_2 Ground state
R_E
R_C
Potential energy
Internuclear distance

FIG. 5

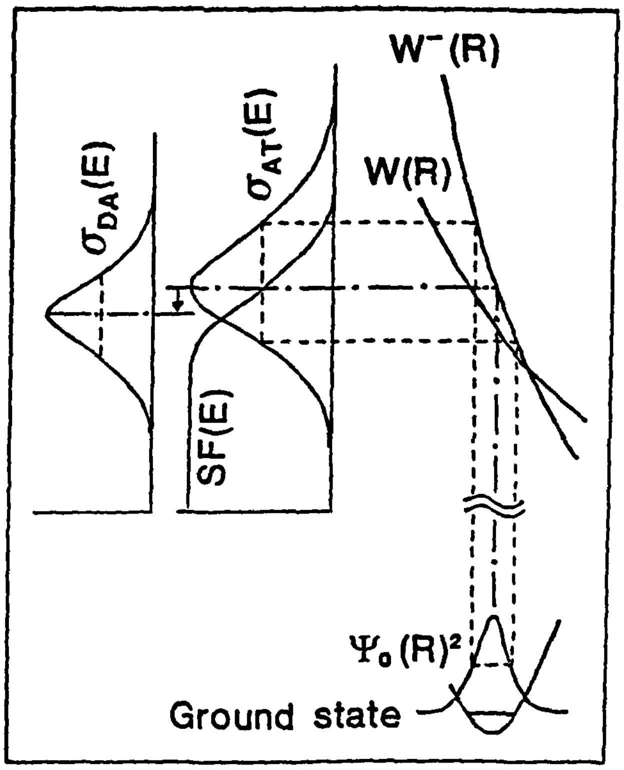

FIG. 6

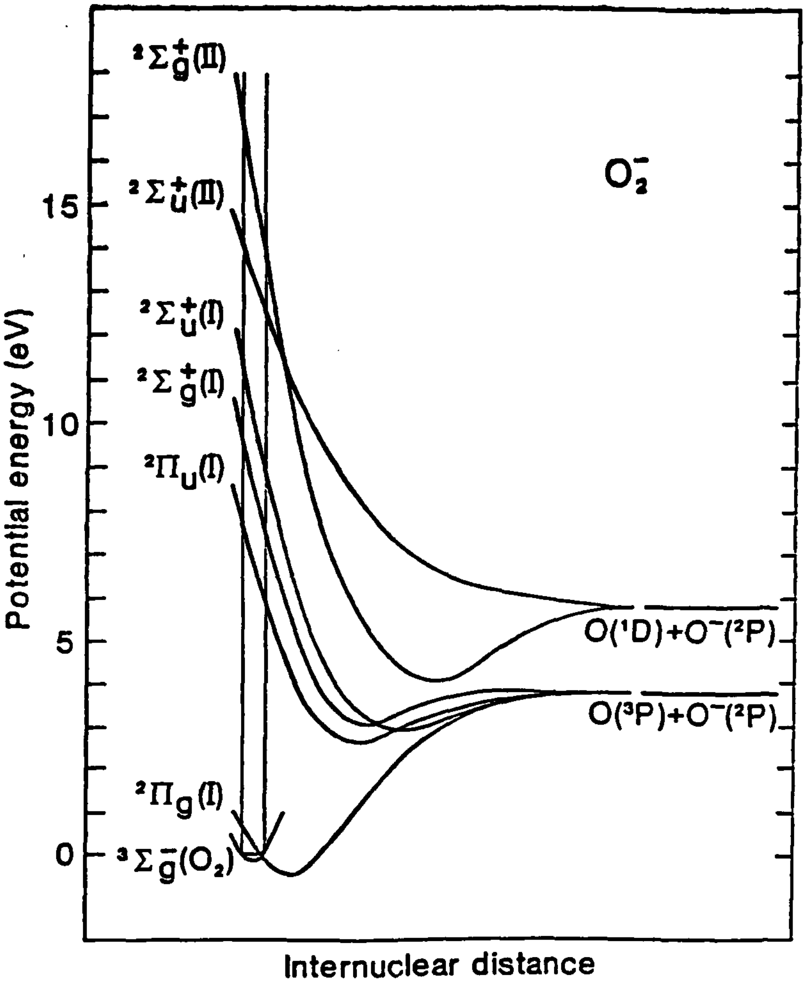
$^2\Sigma_g^+(\mathrm{II})$
$^2\Sigma_u^+(\mathrm{II})$
$^2\Sigma_u^+(\mathrm{I})$
$^2\Sigma_g^+(\mathrm{I})$
$^2\Pi_u(\mathrm{I})$
$^2\Pi_g(\mathrm{I})$
$^3\Sigma_g^-(O_2)$
O_2^-
15
10
5
0
Potential energy (eV)
Internuclear distance
$O(^1D)+O^-(^2P)$
$O(^3P)+O^-(^2P)$

FIG. 7

DL/1113/87/2

TECHNICAL REPORT DISTRIBUTION LIST, GEN

	No. Copies
Office of Naval Research Attn: Code 1113 800 N. Quincy Street Arlington, Virginia 22217-5000	2
Dr. Bernard Douda Naval Weapons Support Center Code 50C Crane, Indiana 47522-5050	1
Naval Civil Engineering Laboratory Attn: Dr. R. W. Drisko, Code L52 Port Hueneme, California 93401	1
Defense Technical Information Center Building 5, Cameron Station Alexandria, Virginia 22314	12 high quality
DTNSRDC Attn: Dr. H. Singerman Applied Chemistry Division Annapolis, Maryland 21401	1
Dr. William Tolles Superintendent Chemistry Division, Code 6100 Naval Research Laboratory Washington, D.C. 20375-5000	1

	No. Copies
Dr. David Young Code 334 NORDA NSTL, Mississippi 39529	1
Naval Weapons Center Attn: Dr. Ron Atkins Chemistry Division China Lake, California 93555	1
Scientific Advisor Commandant of the Marine Corps Code RD-1 Washington, D.C. 20380	1
U.S. Army Research Office Attn: CRD-AA-IP P.O. Box 12211 Research Triangle Park, NC 27709	1
Mr. John Boyle Materials Branch Naval Ship Engineering Center Philadelphia, Pennsylvania 19112	1
Naval Ocean Systems Center Attn: Dr. S. Yamamoto Marine Sciences Division San Diego, California 91232	1

DL/1113/87/2

ABSTRACTS DISTRIBUTION LIST, 056/625/629

Dr. J. E. Jensen
Hughes Research Laboratory
3011 Malibu Canyon Road
Malibu, California 90265

Dr. J. H. Weaver
Department of Chemical Engineering
and Materials Science
University of Minnesota
Minneapolis, Minnesota 55455

Dr. A. Reisman
Microelectronics Center of North Carolina
Research Triangle Park, North Carolina
27709

Dr. M. Grunze
Laboratory for Surface Science
and Technology
University of Maine
Orono, Maine 04469

Dr. J. Butler
Naval Research Laboratory
Code 6115
Washington D.C. 20375-5000

Dr. L. Interante
Chemistry Department
Rensselaer Polytechnic Institute
Troy, New York 12181

Dr. Irvin Heard
Chemistry and Physics Department
Lincoln University
Lincoln University, Pennsylvania 19352

Dr. K. J. Klaubunde
Department of Chemistry
Kansas State University
Manhattan, Kansas 66506

Dr. C. B. Harris
Department of Chemistry
University of California
Berkeley, California 94720

Dr. R. Bruce King
Department of Chemistry
University of Georgia
Athens, Georgia 30602

Dr. R. Reeves
Chemistry Department
Renssaeler Polytechnic Institute
Troy, New York 12181

Dr. Steven M. George
Stanford University
Department of Chemistry
Stanford, CA 94305

Dr. Mark Johnson
Yale University
Department of Chemistry
New Haven, CT 06511-8118

Dr. W. Knauer
Hughes Research Laboratory
3011 Malibu Canyon Road
Malibu, California 90265

Dr. Theodore E. Madey
Surface Chemistry Section
Department of Commerce
National Bureau of Standards
Washington, D.C. 20234

Dr. J. E. Demuth
IBM Corporation
Thomas J. Watson Research Center
P.O. Box 218
Yorktown Heights, New York 10598

Dr. M. G. Lagally
Department of Metallurgical
and Mining Engineering
University of Wisconsin
Madison, Wisconsin 53706

Dr. R. P. Van Duyne
Chemistry Department
Northwestern University
Evanston, Illinois 60637

Dr. J. M. White
Department of Chemistry
University of Texas
Austin, Texas 78712

Dr. Richard J. Saykally
Department of Chemistry
University of California
Berkeley, California 94720

DL/1113/87/2

ABSTRACTS DISTRIBUTION LIST, 056/625/629

Dr. G. A. Somorjai
Department of Chemistry
University of California
Berkeley, California 94720

Dr. J. Murday
Naval Research Laboratory
Code 6170
Washington, D.C. 20375-5000

Dr. W. T. Peria
Electrical Engineering Department
University of Minnesota
Minneapolis, Minnesota 55455

Dr. Keith H. Johnson
Department of Metallurgy and
Materials Science
Massachusetts Institute of Technology
Cambridge, Massachusetts 02139

Dr. S. Sibener
Department of Chemistry
James Franck Institute
5640 Ellis Avenue
Chicago, Illinois 60637

Dr. Arold Green
Quantum Surface Dynamics Branch
Code 3817
Naval Weapons Center
China Lake, California 93555

Dr. A. Wold
Department of Chemistry
Brown University
Providence, Rhode Island 02912

Dr. S. L. Bernasek
Department of Chemistry
Princeton University
Princeton, New Jersey 08544

Dr. W. Kohn
Department of Physics
University of California, San Diego
La Jolla, California 92037

Dr. Stephen D. Kevan
Physics Department
University Of Oregan
Eugene, Oregon 97403

Dr. David M. Walba
Department of Chemistry
University of Colorado
Boulder, CO 80309-0215

Dr. L. Kesmodel
Department of Physics
Indiana University
Bloomington, Indiana 47403

Dr. K. C. Janda
University of Pittsburg
Chemistry Building
Pittsburg, PA 15260

Dr. E. A. Irene
Department of Chemistry
University of North Carolina
Chapel Hill, North Carolina 27514

Dr. Adam Heller
Bell Laboratories
Murray Hill, New Jersey 07974

Dr. Martin Fleischmann
Department of Chemistry
University of Southampton
Southampton SO9 5NH
UNITED KINGDOM

Dr. H. Tachikawa
Chemistry Department
Jackson State University
Jackson, Mississippi 39217

Dr. John W. Wilkins
Cornell University
Laboratory of Atomic and
Solid State Physics
Ithaca, New York 14853

Dr. Ronald Lee
R301
Naval Surface Weapons Center
White Oak
Silver Spring, Maryland 20910

Dr. Robert Gomer
Department of Chemistry
James Franck Institute
5640 Ellis Avenue
Chicago, Illinois 60637

Dr. Horia Metiu
Chemistry Department
University of California
Santa Barbara, California 93106

Dr. W. Goddard
Department of Chemistry and Chemical
Engineering
California Institute of Technology
Pasadena, California 91125

ABSTRACTS DISTRIBUTION LIST, 056/625/629

Dr. F. Carter
Code 6170
Naval Research Laboratory
Washington, D.C. 20375-5000

Dr. Richard Colton
Code 6170
Naval Research Laboratory
Washington, D.C. 20375-5000

Dr. Dan Pierce
National Bureau of Standards
Optical Physics Division
Washington, D.C. 20234

Dr. R. G. Wallis
Department of Physics
University of California
Irvine, California 92664

Dr. D. Ramaker
Chemistry Department
George Washington University
Washington, D.C. 20052

Dr. J. C. Hemminger
Chemistry Department
University of California
Irvine, California 92717

Dr. T. F. George
Chemistry Department
University of Rochester
Rochester, New York 14627

Dr. G. Rubloff
IBM
Thomas J. Watson Research Center
P.O. Box 218
Yorktown Heights, New York 10598

Dr. J. Baldeschwieler
Department of Chemistry and
Chemical Engineering
California Institute of Technology
Pasadena, California 91125

Dr. Galen D. Stucky
Chemistry Department
University of California
Santa Barbara, CA 93106

Dr. A. Steckl
Department of Electrical and
Systems Engineering
Rensselaer Polytechnic Institute
Troy, New York 12181

Dr. John T. Yates
Department of Chemistry
University of Pittsburgh
Pittsburgh, Pennsylvania 15260

Dr. R. Stanley Williams
Department of Chemistry
University of California
Los Angeles, California 90024

Dr. R. P. Messmer
Materials Characterization Lab.
General Electric Company
Schenectady, New York 22217

Dr. J. T. Keiser
Department of Chemistry
University of Richmond
Richmond, Virginia 23173

Dr. R. W. Plummer
Department of Physics
University of Pennsylvania
Philadelphia, Pennsylvania 19104

Dr. E. Yeager
Department of Chemistry
Case Western Reserve University
Cleveland, Ohio 41106

Dr. N. Winograd
Department of Chemistry
Pennsylvania State University
University Park, Pennsylvania 16802

Dr. Roald Hoffmann
Department of Chemistry
Cornell University
Ithaca, New York 14853

Dr. Robert L. Whetten
Department of Chemistry
University of California
Los Angeles, CA 90024

Dr. Daniel M. Neumark
Department of Chemistry
University of California
Berkeley, CA 94720

Dr. G. H. Morrison
Department of Chemistry
Cornell University
Ithaca, New York 14853